All-Atom Simulation Method for Zeeman Alignment and Dipolar Assembly of Magnetic Nanoparticles

*Akhlak U. Mahmood and Yaroslava G. Yingling**

Email: yara_yingling@ncsu.edu

Department of Materials Science and Engineering, NC State University, Raleigh, NC 27695, U.S.A.

ABSTRACT

Magnetic nanoparticles (MNPs) can organize into novel structures in solutions with excellent order and unique geometries. However, studies of the self-assembly of smaller MNPs are challenging due to a complicated interplay between external magnetic fields and van der Waals, electrostatic, dipolar, steric, and hydrodynamic interactions. Here, we present a novel all-atom molecular dynamics (AMD) simulation method to enable detailed studies of the dynamics, self-assembly, structure and properties of MNPs as a function of core sizes and shapes, ligand chemistry, solvent properties and external field. We demonstrate the use and effectiveness of the model by simulating the self-assembly of oleic acid ligand-functionalized magnetite (Fe_3O_4) nanoparticles, with spherical and cubic shapes, into rings, lines, chains, and clusters under a uniform external magnetic field. We found that the long-range electrostatic interactions can favor

the formation of a chain over a ring, the ligands promote MNP cluster growth, and the solvent can reduce the rotational diffusion of the MNPs. The algorithm has been parallelized to take advantage of multiple processors of a modern computer and can be used as a plugin for the popular simulation software LAMMPS to study the behavior of small magnetic nanoparticles and gain insights into the physics and chemistry of different magnetic assembly processes with atomistic details.

Keywords: all-atom molecular dynamics, magnetic nanoparticles, ligands, dipolar assembly, effects of chemistry

INTRODUCTION

Magnetic nanoparticles (MNPs) carry a permanent magnetic dipole moment that dictates the magnetic properties of the particles and the responsiveness of the particles to an externally applied magnetic field. The origin of the magnetic dipole moment is primarily due to the spin imbalance of the 3d orbital electrons of transition metals, such as Fe, Ni, and Co, that are present as oxides or alloys in the inorganic core of the MNPs.[1,2] Single MNPs can be of different shapes and sizes (spheres, cubes, ellipsoids, *etc*.) and spontaneously self-assemble, due to the anisotropic nature of the dipole-dipole (d-d) interactions, into larger novel aggregates in colloidal solutions with extraordinary ordering and interesting geometries such as rings, wires, lines and chains.[3] Since the magnetic properties of the particles depend solely on the strength and orientation of the embedded dipole moments, the main advantage of MNPs over non-magnetic counterparts is in the control over their dynamics and self-assembly using magnetic fields in various *in-situ* and *in-vivo* environments. Successful manipulations of MNPs have been demonstrated for a wide range of applications in magnetic particle imaging, magnetic

hyperthermia, targeted drug delivery, lithography, high-density data storage, actuation, sensing and nanorobotics.[4–10]

The dynamical and physical properties of MNPs are defined by various thermodynamic parameters at the nanoscale, and the presence of magnetic dipole moments adds another level of difficulty to the study of the self-assembly of the particles. For example, the strength of the magnetic interaction directly depends on the volume of the magnetic core; a larger colloidal particle with a size greater than 100 nm contains multiple magnetic domains, while a smaller nanoparticle with a size less than 100 nm can be superparamagnetic and a stable single domain, carrying only one magnetic dipole moment.[11] Another important parameter is the MNP shape that impacts the formation of the structure of aggregates. For example, the formation of chain and flux closure rings is a well-known, characteristic phenomenon of spherical MNPs.[12–17] In a recent study, Taheri *et al.* experimentally investigated the size and shape dependence of the field-induced assembly of oleic acid-stabilized cubic Fe_3O_4 MNPs in toluene.[18] They found that cubic particles must be at least 7.5 nm to generate a large enough dipolar force that can align the particles along the magnetic field overcoming thermal and viscous energy barriers, whereas the spherical MNPs must be at least 10 nm in diameter to assemble into 1D chains. Additionally, modern synthetic technologies have allowed researchers to produce non-spherical MNPs with tunable shapes (and anisotropy) such as cubes, rods, peanuts and ellipsoids that can create lines, 2D lattices, and helical ropes with interesting geometries.[19,20] In particular, the cubic MNPs have gained much interest due to their high directionality and ability to form virtually defect-free superstructures with excellent order and packing fractions.[21–23] Moreover, the application of external fields can greatly improve the stability of the formed superstructures. For example, chains formed by 15-nm spherical Co MNPs were reported to stay stable under the influence of

an external magnetic field; however, when the field was removed, the chains became floppy and sedimented in solution. Finally, a complete rotation of the chains was observed when the direction of the external magnetic field was reversed, underscoring the effect of a strong d-d interaction between the Co MNPs.[24] In another study, bidirectional chains were formed by concurrent applications of electric and magnetic fields due to the presence of both electric and magnetic dipole moments in the superparamagnetic 5.7-μm colloidal particles stabilized by carboxylate ions; however, the morphology of the equilibrium assembly was found to be dynamic and highly sensitive to the concentration and initial configuration of the particles.[25] While the diversity of MNP properties permits flexible ways to yield various interesting structures, a deeper understanding of the correlation between structure, dynamical properties, environment and phase behavior is needed.

Other important and correlated parameters that have not been explored in much detail are ligands and solvent environment. The stability of MNPs depends on solvent and ligands, while the solvent additionally determines the responsiveness of the MNPs to an external magnetic field.[26] Past studies have shown that the deviation from the Stokes-Einstein theory of diffusion applied to MNPs is significant when particle-solvent interactions are high, and changes in size and surface energy drastically affect the translational and rotational diffusions of the colloidal MNPs.[26–28] In these studies, it was found that rough particle surfaces contribute to the significant enhancement of local viscosity and packing at the nanoscale, which gets augmented with interactions between the ligands and solvent.[29] The presence of ions creates additional difficulties since the ions can have effects on the interparticle interaction and change the final pattern in colloidal structures.[22,30] Furthermore, the presence of binary mixtures or interfaces poses an additional challenge due to induced solvent interactions.[31] On the other hand, to attain

colloidal stability, the core of the MNP usually needs to be passivated by ligands such as oleic acid, oleylamine, polyethyleneimine, polyethylene glycol, diethylene glycol, thiols, or ions.[32–36] The chemistry and structure of ligands influence the effective size of the particles, the maximum magnetic dipolar interaction possible between two particles, and properties of applied MNP-based materials, such as physicochemical stability and biological fate.[37] Surface-bound ligands can also alter the magnetic dipole moments of MNPs by introducing spin disorders in the surface atoms.[38] However, the effects of ligands on the dynamics of MNPs and the assembled structure are still not fully understood.[17,30,39] For example, the absence of long-range order, investigated via scanning electron microscopy and Monte Carlo (MC) simulations, of spherical γ-Fe_2O_3 MNPs was attributed to anisotropy of the dipole moments and ligand properties in 2D arrays of the particles.[40] It has been suggested that tuning the capping ligands could provide MNPs with the ability to form structures with enhanced long-range order in solvents, due to a reduction of entropy when two particles approach each other.[41] Overall, the intricate interplay between various MNP system components, such as the magnetic core, the ligands, the local solvent environment of the MNPs and external stimuli makes the understanding of how to control MNP systems difficult to unravel.

Analytical and computational methods have been extensively utilized to resolve the complexities of MNPs and to predict the equilibrium structures formed by such particles. A commonly employed *in-silico* representation of MNPs is a dipolar hard sphere model, or variations thereof, where a point dipole is located at the center of the particles.[42] This simple model has been particularly successful in the prediction of the aggregated structure and phase behaviors of magnetic colloidal systems with different sizes, shapes, and dipolar positions. For example, earlier studies using this model with standard MC, Brownian dynamics, and coarse-

grained (CG) molecular dynamics (MD) simulations have investigated spherical MNPs, where ring and chain formations in magnetic fluids were attributed to the strong anisotropy of the dipolar force and a preference for the *head-to-tail* arrangements of the dipole moments of the particles.[43–45] Later studies focused on more complex systems, such as the assembly of 8,000 spherical colloidal particles under a dipolar potential using Langevin dynamics[46] and the effects of solvent evaporation using quasi-2D MC simulations.[47] Additionally, CG-MD simulation techniques were used to decipher the influence of dipolar interactions on magnetic imaging technologies in time-dependent magnetic fields[48] and the hydrodynamics of red blood cells under an externally rotating magnetic field[49]. Using coarse-grained cubic and spherical structures and magnetic dipolar approximation[50,51], Donaldson and Kantorovich showed that magnetic flux closure ring formation is favorable only in the case of spherical nanoparticles.[52] The effect of magnetic anisotropy on superstructure formation by dipolar alignments in the [111] and [100] crystallographic directions in cubic MNPs was studied using coarse-grained MC modeling techniques, where a [111] direction-oriented superstructure was found to be favored above a certain MNP concentration.[53] Ion-stabilized magnetic nanocubes were found to assemble on their corners using a CG-MD technique that included surface area, surface binding energy, and dipolar elements.[22] In most computational studies, however, surfactants are largely ignored or approximated by mesoscale simulation methods, and the solvent is represented by a homogeneous continuous function with no explicit chemistry or long-range hydrodynamic interactions.[31] However, ligands were shown to be responsible for helical rope formation by 5-nm cubic MNPs using MC simulations in a drying-mediated self-assembly environment (solvent not present).[20] Therefore, the complex interplay of explicit chemical interactions between MNP

ligands and solvent at the nanoscale may lead to the otherwise unexplained formation of unusual geometries.

Overall, a new computational method is needed for MNP systems for several reasons. First, at the nanoscale, the size of the solvent molecules becomes comparable to that of MNPs, and continuum approximation of the solvent fails. As a result, the models that are suitable for the mesoscale and microscale become inefficient for smaller MNPs, as the separation of length and time scale of the particles and the solvent molecules is no longer possible.[54] Second, the local packing of solvent molecules and ions around an MNP core and ligand layer can change the pairwise inter-particle interactions, diffusivity, and effective radius of the particles, which drastically affects the morphology and phase behavior of the final structures produced by the MNPs.[29,44] Hence, for an MNP with a size in the nanometer range, the solvent molecules must be simulated explicitly and ligands must be accounted for. Third, magnetic dipolar strength becomes significantly weaker for magnetic cores with smaller sizes. At the nanoscale, the magnetic interaction energies of the MNPs often become comparable to the short-range van der Waals (VDW) and steric forces and thermal energy of the particles due to the presence of an internal structure and ligands and vibration of atoms. Similarly, the magnitude of the long-range hydrodynamic forces due to solvent, and electrostatic forces, surface energy due to a net charge of the MNPs reduce significantly. Coupling of the short-range and long-range forces and the interplay of shape anisotropy and the magneto-crystalline anisotropy can create unique structures such as the helical ropes and the diagonal assembly of cubic MNPs as noted earlier.[20,22] All-atom MD can overcome most of the nanoscale-associated challenges by modeling the explicit chemistry of the MNP core, ligands, and solvents with atomic-level details, hence eliminating the need for many approximations typically adopted in mesoscale models.

Here, we describe a novel explicit solvent all-atom MD simulation model to simulate the behavior of MNPs due to Zeeman interaction under the influence of an external magnetic field and dipolar interaction. In this model, the nanoparticles are assumed to have a magnetically hard, rigid core, optionally coated with ligands. The dynamics of the magnetic core are evaluated as a rigid body composed of a distribution of atoms, whereas the ligands and surrounding solvent interactions are simulated with full atomic-level details. This hybrid approach allows us to simulate the dynamics of complex MNPs in any environment while maintaining a high resolution and fidelity. We estimate that this atomistic model can be used to simulate magnetic interactions of MNP systems with a particle size of up to 30 nm and a hundreds-of-nanoseconds timescale using current computational resources. To demonstrate the accuracy and capabilities of the proposed model, we chose Fe_3O_4 MNPs as a model material due to a plethora of available experimental studies.[55] Specifically, we examined MNP systems with bare and oleic acid ligand-coated spherical and cubic Fe_3O_4 MNPs and simulated the formation of dipolar line, ring, cluster, chain, and staggered-chain structures (**Figure 1** (a, b)). Our findings, the effects of simulation parameters, and advantages and limitations of the proposed model are discussed in detail below.

RESULTS AND DISCUSSION

Magnetic Nanoparticle Model

We consider a single-domain, magnetically hard, spherical nanoparticle carrying a net magnetic dipole moment $\vec{m}$.

To represent the dipole moment $\vec{m}$ inside a spherical nanoparticle core of size d, we choose two existing atoms at positions $\overrightarrow{X_1}$ and $\overrightarrow{X_2}$ on an arbitrary diameter vector, $\vec{d}$, across the core (**Figure 1** (a)). We assign the selected two atoms a new *atomtype*, "*Ms*", and a 'magnetic charge'

parameter, $|q_m|$, while keeping the rest of their MD force field parameters unchanged. The new *atomtype* allows us to easily keep track of the selected two atoms during the simulation without affecting their chemical interactions. Additionally, by setting positive and negative values of 'magnetic charge' q_m, each of the two *Ms* atoms can be uniquely identified. The q_m 'magnetic charge' parameter is independent of the atomic partial charge and does not contribute to any interatomic interactions of the *Ms* atoms and only used to determine the position and direction of the dipole moment. The dipole moment vector $\vec{m}(t)$ at time t can then be defined as,

$$\vec{m}(t) = \beta\,|q_m|\,\vec{d} = \beta\,|q_m|\,\left(\overrightarrow{X_2}(t) - \overrightarrow{X_1}(t)\right) \qquad (1)$$

where β is a scaling factor to adjust the magnitude of the dipole moment, if necessary. At each integration time step, the position and orientation of the dipole moment $\vec{m}(t)$ can be determined using Equation (1).

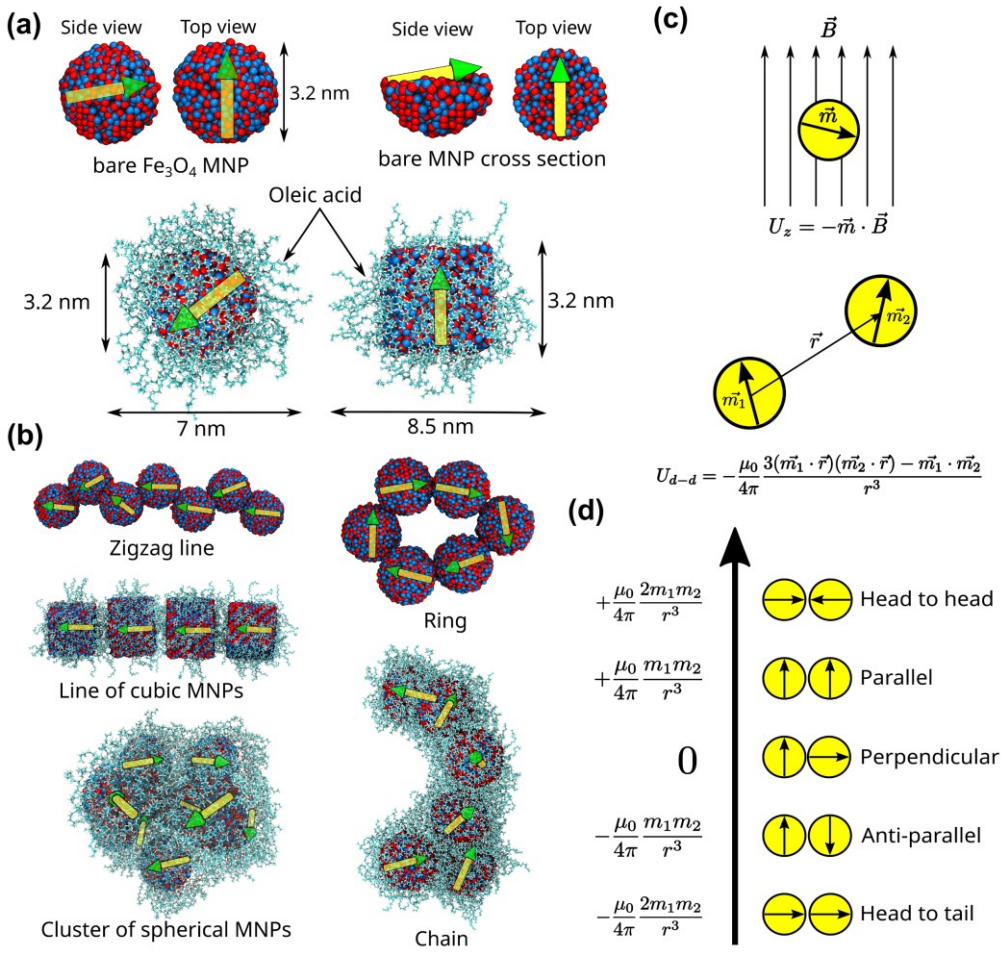

Figure 1. (a) Models of the magnetic Fe_3O_4 nanoparticles used in all-atom MD simulations, showing the set-up of an embedded magnetic dipole moment in the MNP core. (b) Representative snapshots of the self-assembled structures obtained in all-atom MD simulations with dipole vectors (transparent arrows), iron atoms (dark blue), oxygen atoms (dark red), and oleic acid ligand molecules (cyan). (c) Schematic representations of possible Zeeman and dipolar interactions of spherical MNPs. (d) Five characteristic configurations of two self-assembled spheres due to the anisotropy of their dipolar interaction. The interaction energy gradually increases from the most attractive *head-to-tail* configuration to the most repulsive *head-to-head* configuration.

Figure 1 (a) shows the side view, top view, and the cross-section of a 3.2-nm bare spherical Fe_3O_4 nanoparticle used in this work. The orientation and position of the dipole moment are shown by the transparent arrow, where the green arrowhead shows the direction of the dipole

moment. Oleic acid ligand-coated 7-nm spherical and 8.5-nm cubic MNPs are shown in the following row. In this model, the 3-nm spherical and cubic Fe_3O_4 nanoparticle core contains 1,622 and 3,580 covalently bonded atoms, respectively. The distance between the core atoms always stays constant, while the core translates and rotates as a rigid body. Thus, the magnitude of $\vec{m}(t)$ remains the same independent of the core's orientation. Once the dipole moment is defined, the corresponding Zeeman energy of the dipole in an external magnetic field, $\vec{B}$, is given by the Equation,

$$U_Z = -\vec{m} \cdot \vec{B} \tag{2}$$

Then, the d-d interaction energy between two MNPs is defined by,

$$U_{d-d} = -\alpha \frac{\mu_0}{4\pi} \frac{3\,(\vec{m_1}\cdot\vec{r})(\vec{m_2}\cdot\vec{r}) - \vec{m_1}\cdot\vec{m_2}}{r^3} \tag{3}$$

where $\vec{m_1}$ is the dipole moment of particle 1, $\vec{m_2}$ is the dipole moment of particle 2, $\vec{r}$ is the center-of-mass to center-of-mass distance vector from particle 1 to particle 2, μ_0 is the vacuum permeability, and α is a dipolar energy scaling factor that may arise due to the short distance correlation between the dipole moments[56], the geometry of the particles[57] and the relative permeability of the surrounding medium. The range of dipole-dipole interaction dies off quickly as a function of distance by r^{-3} where the long-range Coulombic interaction decays by r^{-1}. It has been shown previously that the higher-order terms due to the finite-size effects of the particle decay by r^{-5}.[58] Hence, we can ignore the finite-size effects of the particles.

Figure 1 (c) shows the schematic representations of magnetic Zeeman and dipolar interactions. U_Z depends on the orientation of the embedded dipole moment relative to the direction of the applied magnetic field. The torque exerted on the dipole due to Zeeman interaction is $\vec{\tau_Z} = \vec{m} \times \vec{B}$, and the exerted force is $\vec{F_Z} = \vec{m} \cdot \vec{\nabla}\,\vec{B}$. In a homogenous uniform magnetic field, however, the force term vanishes. In contrast, the torque term is non-zero, and the core of the

nanoparticle rotates itself towards the direction of the applied field to minimize the magnetic Zeeman interaction energy defined by Equation (2). Additionally, the dipolar interaction torques and forces are given by, [59]

$$\overrightarrow{\tau_{12}} = \alpha \frac{\mu_0}{4\pi}\left[\frac{3}{r^5}(\overrightarrow{m_2}\cdot\vec{r})(\overrightarrow{m_1}\times\vec{r}) - \frac{1}{r^3}(\overrightarrow{m_1}\times\overrightarrow{m_2})\right]$$

$$\overrightarrow{\tau_{21}} = \alpha \frac{\mu_0}{4\pi}\left[\frac{3}{r^5}(\overrightarrow{m_1}\cdot\vec{r})(\overrightarrow{m_2}\times\vec{r}) - \frac{1}{r^3}(\overrightarrow{m_2}\times\overrightarrow{m_1})\right] \quad (4)$$

$$\vec{F}_{d-d} = \alpha \frac{\mu_0}{4\pi}\left[\frac{3}{r^5}(\overrightarrow{m_1}\cdot\overrightarrow{m_2})\vec{r} - \frac{15}{r^7}(\overrightarrow{m_1}\cdot\vec{r})(\overrightarrow{m_2}\cdot\vec{r})\vec{r} + \frac{3}{r^5}\{(\overrightarrow{m_2}\cdot\vec{r})\overrightarrow{m_1} + (\overrightarrow{m_2}\cdot\vec{r})\overrightarrow{m_1}\}\right]$$

where $\overrightarrow{\tau_{12}}$ is the torque exerted on particle 1 by the dipole moment of particle 2, and $\overrightarrow{\tau_{21}}$ is the torque exerted on particle 2 by the dipole moment of particle 1. Due to the inherent anisotropy of the dipolar interactions, five typical configurations of two self-assembled spherical MNPs can be identified, as shown in **Figure 1** (d). The most favorable configuration is the *head-to-tail* configuration of the two dipole moments corresponding to the lowest dipolar energy value. The next favorable configuration is the *anti-parallel* configuration, where the dipole moments of the particles face opposite directions. The *perpendicular* configuration of the dipole moments is neither favorable nor unfavorable due to a vanishing dipolar energy. The *parallel* dipolar configuration is generally unfavorable. Lastly, the *head-to-head* configuration is the most repulsive dipolar configuration and usually not observed in experimental MNP systems.

All-atom MD Simulation Method

The magnetic core of the colloidal MNPs contains a large number of harmonically bonded atoms that move together as a rigid body in solution, an approach that we successfully used for all-atom simulations of gold NPs.[60–62] If the particle is magnetically hard, magnetic dipolar interactions and an external magnetic field exert additional forces to drive the movement of the rigid core such that the relative positions of the core atoms remain constant, and the atoms move together as a single entity. Therefore, a simple and direct approach to attain atomistic details of

the MNP magnetic core in an all-atom MD simulation is to treat the core as a rigid body. In the case of atomistic simulations, such methods have been used to constrain the high frequency motions of atoms in small molecules using algorithms such as SHAKE[63] and RATTLE[64] that allow longer time steps and an increased speed of the simulations. For larger rigid particles, many time-reversible and symplectic algorithms for rigid-body dynamics have been developed.[54,65,66] [67] In our model, the forces and torques exerted on the magnetic core of the MNP are calculated as the sum of the respective terms experienced by the magnetic dipole moments of the core, an approach similar to one described in Ref. [67]. Given the presence of a dipole moment defined by Equation (**Error! Reference source not found.**) embedded in the MNP core, the magnetic dipolar force and torques can be calculated for the rigid core by Equation (4), and in an external magnetic field, the forces due to Zeeman interactions can be similarly computed. Moreover, the surface of such a particle is still represented by an all-atom representation, and ligand molecules with all-atom details can be covalently attached to the atoms on the surface of the core. In addition, ligands can independently move and exert additional forces on the core. The ligand functionalized MNP then consequently experiences a net force that is the sum of all magnetic interactions due to the magnetic dipole moments, chemical interactions with solvents, and other thermodynamic interactions on the core. In that way, the dynamics of the MNP are captured without any further approximations.

Therefore, using Equations (2) and (3) we get the following modified Hamiltonian of an MNP system implemented in the model.

$$U_{total} = \sum_{bonds} k_b(r - r_0)^2 + \sum_{angles} k_\theta(\theta - \theta_0)^2 + \sum_{dihedrals} V_n[1 + cos(n\phi - \gamma)]$$

$$+ \sum_{i=1}^{N-1} \sum_{j=i+1}^{N} \left[\frac{A_{ij}}{R_{ij}^{12}} - \frac{B_{ij}}{R_{ij}^{6}} + \frac{q_i q_j}{\epsilon R_{ij}}\right] - \sum_{i=1}^{M} \vec{m}_i \cdot \vec{B}$$

$$- \sum_{i=1}^{M-1} \sum_{j=i+1}^{M} \alpha \frac{\mu_0}{4\pi} \frac{3(\vec{m}_i \cdot \vec{r}_{ij})(\vec{m}_j \cdot \vec{r}_{ij}) - \vec{m}_i \cdot \vec{m}_j}{r_{ij}^3}$$

where, N is the number of atoms, M is the number of magnetic dipole moments, $k_b, r_0, k_\theta, \theta_0, V_n, \gamma, A_{ij}, B_{ij}$ are all-atom force field parameters,[68] q_i, q_j are atomic partial charges, $\vec{m}_i$, $\vec{m}_j$ are the magnetic dipole moments calculated using Equation (1), and $\vec{B}$ is the external time-invariant magnetic field applied to the system. The magnetic terms are calculated and applied only to the rigid magnetic cores of the MNPs that follow the rigid body dynamics discussed before. Additionally, the dipolar and the external magnetic field interactions are simulated by modifying the total energy of the cores. However, it is important to note that, in our model, the externally applied magnetic field needs to be time-invariant, so that in the absence of any free currents and any time-varying electric fields, the curl of the magnetic field vanishes, (*i.e.*, $\vec{\nabla} \times \vec{B} = 0$), and the force produced by the applied magnetic field is conservative. In such a system, the Hamiltonian also remains conservative,[69] and the long-term dynamical evolution of the system can be calculated using a time-reversible symplectic integrator.[70] In addition, in an external magnetic field, a charged particle moving with velocity $\vec{v}$, experiences a Lorentz force given by $\vec{F}_L = q \cdot (\vec{v} \times \vec{B})$, where q is the charge of the particle. However, velocity-dependent forces are non-conservative and to simulate the resulting dynamics, a modification of the force during the half-timestep of the integration algorithm is required, which is not supported by the

Velocity-Verlet algorithm.[71] We, therefore, ignore the effects of the Lorentz force in the present model for the sake of simplicity.

Choice of Simulation Systems

In this work, four characteristic MNP systems were simulated to demonstrate the applicability and performance of the proposed model (Table S1):

(1) To begin with the simplest system possible, we studied the effects of an external magnetic field on the Zeeman rotation and alignment of a single bare MNP in hexane and ethanol solvents while keeping the dipolar interactions turned off. Numerous past studies using mesoscale simulation methods have systematically investigated the rotational diffusion of MNP systems to investigate critical size, ligands, surface energy and roughness, and viscosity of the solvents.[26,27,29,72] We qualitatively reproduced such dynamics and additionally report the importance of the surface charge density of the bare MNP and solvent polarity on the Zeeman rotation of the particle.

(2) We then focus on the dipolar interaction only and simulate the assembly of eight spherical MNPs in vacuum without the presence of any external magnetic field. The particular choice of this system was inspired by multiple recent studies on the dipole-induced cluster formation by eight nanoparticles where an infinite number of possible ground state configurations was predicted using analytical methods.[73,74]

(3) In the case of multiple cubic nanoparticles, perfectly linear straight lines of MNPs can form due to shape anisotropy. This system is especially complex since both dipolar and external field interactions are present in the system. To demonstrate such shape anisotropy effects, the ability to easily build particles with different geometries, and inspired by experimental works on cubic MNPs by Taheri *et al.*,[18] we simulated line formation by cubic MNPs in hexane in the presence

of a uniform external field. The interplay of surfactants and external field interactions and the mechanism of assembly of the particles are obtainable.

(4) Finally, ring formation due to strong dipolar interactions by four or more spherical MNPs is a characteristic phenomenon. Moreover, for a finite number of particles, ring formation is more favorable than line formation by the MNPs.[75] We therefore simulated chain and ring formation by eight spherical MNPs to validate the model. The details of the thermodynamic conditions, initial setup of the particles, model parameters and results for the MNP systems are discussed in the following individual sections.

Zeeman Rotation of Bare MNPs in an External Uniform Magnetic Field

To test the importance of surface charge density on particle dynamics under an external magnetic field, four independent simulation systems with a single solvated bare-MNP were employed. In two of the systems, a charge-neutral bare magnetic particle model was solvated in either ethanol or hexane. In the other two systems, the MNP with a net surface charge density of +0.05 C/m^2 was solvated in either ethanol or hexane. In all simulations, a single MNP was placed in the center of a simulation box, and its dynamics under the influence of a uniform 1 T magnetic field were examined within 5 ns of simulated time. We observed that the dipole moment of a 3.2-nm Fe_3O_4 nanoparticle was not strong enough to overcome the thermal energy barrier under the influence of a 1 T magnetic field. Thus, a value of the dipole moment scaling factor of $\beta = 5.0$ was set to induce Zeeman rotation. Additionally, dipole-dipole interaction was absent in the systems; therefore, any d-d effects across the periodic boundaries can be ignored in the simulations. Representative snapshots of the simulated system of the charged-neutral MNP solvated in hexane are shown in **Figure 2** (b). The initial angle between the dipole moment embedded inside the MNP and the direction of the applied magnetic field was approximately 160

degrees. The magnetic field introduced a torque on the particle due to magnetic Zeeman interactions as described by Equation (2), while no Zeeman force was experienced by the particle

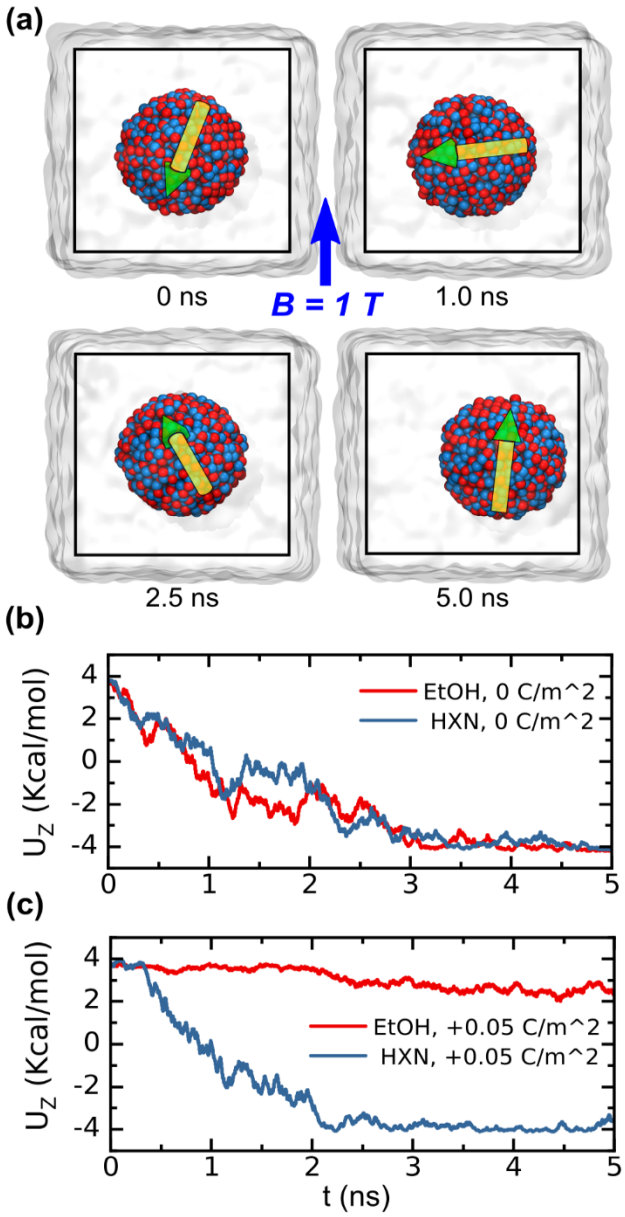

Figure 2. (a) Snapshots of the rotation of a bare charge-neutral Fe_3O_4 nanoparticle under the influence of an external uniform magnetic field. Hexane molecules are shown as the transparent surface; the direction of the dipole moment of the MNP is shown by the transparent arrow, and the uniform magnetic field direction is denoted by the blue arrow (+y direction). Here, the scaling factors were set as $\alpha = 1.0, \beta = 5.0$. (b) Temporal evolution of the Zeeman interaction energy of a charged magnetic nanoparticle (surface charge density +0.05 C/m^2). (c) Temporal evolution of the Zeeman interaction energy for the charge-neutral magnetic particle shown in (a).

due to the absence of a field gradient. As can be seen in the snapshots, the particle rotated towards the direction of the applied field to minimize the magnetic Zeeman energy, U_z. Slight translation of the particle can also be seen in the snapshots due to thermal and Brownian effects. An equilibrium condition was reached when the angle between the direction of the applied field and the dipole moment of the particle reached approximately zero. During the magnetic alignment process, the MNP rotated as a rigid body, while the surface atoms of the bare particle retained their atomistic details and interacted with the surrounding solvent molecules.

A detailed comparison between the four simulated systems can be made by observing the evolution of the interaction energy of the dipole moment with the applied magnetic field. The time evolution of the magnetic Zeeman interaction energies is plotted in **Figure 2** (b, c). We notice that the Zeeman energy values decrease rapidly in the case when the particle had a zero net surface charge. Moreover, this trend was independent of the solvent. The energy loss due to the decrease in Zeeman energy is gained by the rotational kinetic energy of the MNP. This increased kinetic energy overcomes the thermal and viscous energy barrier to facilitate the rotation. No distinguishing effect of ethanol or hexane can be seen from the curves. However, the addition of the surface charge to MNPs allows one to account for solvent properties, as can be seen in the energy plots in the case of charged MNPs in **Figure 2** (b). A decay of the Zeeman energy can be observed in hexane contrary to that of ethanol. In ethanol, only a slight decrease of the Zeeman energy can be observed during the simulations. Thus, we conclude that if the solvent-particle interaction energy is higher than the energy gained by the Zeeman rotation, the alignment of the particle is no longer favorable. Two important parameters should be considered in the case of the MNP in ethanol: solvent-MNP interaction energy and solvent viscosity. A net surface charge density on the surface of the bare MNP causes the particle to favorably interact

with ethanol. Furthermore, for the MNP rotation to occur, the surrounding solvent molecules must be displaced. Ethanol has a higher viscosity than hexane due to the formation of hydrogen bond networks.[76] Thus, the MNP experiences a higher energy barrier during the rotation process in ethanol. Moreover, the effects of the solvents can be quantified by calculating the rotational diffusion constants of the MNP for the four systems. The diffusion constants and the radial distribution functions of the solvent molecules around the MNP are plotted in **Figure S1** and **Figure S2**. It is important to note that long-range electrostatic interaction can also affect the particle rotation.[29] While for the charge-neutral systems, such an effect is non-existent, for the charged MNP systems, we used a large solvent buffer of 50 Å to minimize such long-range effects. Indeed, we observed that, the charged MNP experienced slow rotation when the simulation was conducted with smaller than 15 Å solvent buffer.

Dipolar Assembly of Eight MNPs in Vacuum

To demonstrate the usability of our method for simulations of MNP self-assembly, a simulation with eight oleic acid ligand-coated, charge-neutral, spherical MNPs was used (**Figure 3** (a)). This system is of particular interest because it has been shown that the smallest stable cluster of magnetic spheres generally contains eight particles that form two closed loops (or rings) of the dipoles and creates a perfect symmetrical structure.[73] In our system, initially each MNP was within at least 90 Å apart from their nearest neighbors. The system was then simulated in vacuum in the absence of any external magnetic fields. The MNPs initially started to aggregate with their closest neighbors. At 1.0 ns, a cluster-like structure began to form. By 4.0 ns, a stable cluster of the eight MNPs is obtained. A closer look at the cluster revealed two distinct dipolar rings — one within the four MNPs at the front side in the snapshot, and another dipolar ring within the other four MNPs at the back (**Figure 3** (a), snapshot at 4.0 ns).

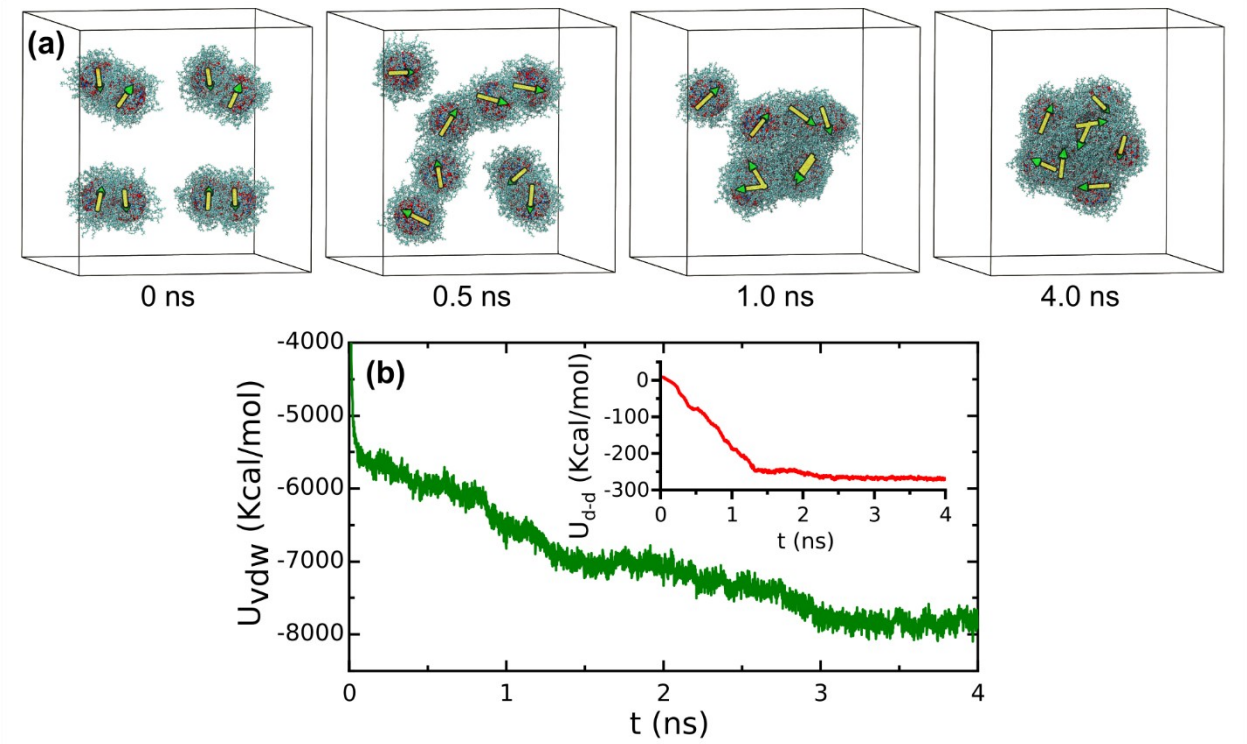

Figure 3. (a) In-vacuo simulation snapshots of eight oleic acid-coated spherical Fe_3O_4 MNPs forming a cluster due to dipolar interactions. A stable double-ring dipolar configuration is obtained after 4 ns. The orientations of both rings are in the clockwise direction indicating failure to reach the ground state configuration. The initial nearest-neighbor separation between the MNPs is 90 Å ($\alpha = 10, \beta = 16.83$). No external magnetic field was applied. (b) Corresponding temporal evolution of the total VDW interaction energy between the interacting ligands and (inset) the dipolar interaction energy of the eight MNPs.

By comparing the VDW and dipolar interaction energies (**Figure 3** (b)), we note that the VDW energy is at least an order of magnitude stronger than the dipolar interaction energy. When the nucleation of the cluster begins, the dipole-dipole interaction of the MNPs competes with the interaction between the oleic acid ligands. Finally, a cluster with a dipolar double-ring configuration is obtained. As can be observed from the convergence of the energy graphs, the final cluster configuration is stable.

Double-ring formation within clusters formed by 14 or more magnetic spheres has been previously predicted using numerical methods.[75] Recently, Hartung *et al.* investigated the ground state configuration of eight magnetic spheres using analytical and numerical techniques.[74] They reported a stable double ring-like configuration of the magnetic dipoles, where an infinite number of orientations of the dipoles is possible in the ground state, provided that the dipoles are free to rotate. A simple way to identify such a stable configuration is that the ring on one side of the cluster faces in the opposite rotational direction of the opposite side of the cluster, for example, one ring on the front side of the cluster rotates in the clockwise direction and another in the back rotates in the anticlockwise direction. This is a consequence of the combination of both favorable *head-to-tail* and *anti-parallel* configurations of the dipoles shown in **Figure 1** (d). In contrast, two rings orienting in the same rotational direction would be the result of the *head-to-tail* and *parallel* configurations and not favorable. A schematic representation of the ground state configuration and top and side views of the dipolar rings obtained in the simulation are shown in **Figure S3**. Hartung *et al.* further showed that, in the favorable ground state, the magnetic flux density outside the cluster drastically decreases by r^{-7} creating a stable assembly of the spheres and preventing further growth of the cluster solely due to magnetic interaction. In our simulated system, however, all-atom MD did not obtain the ground state configuration of the dipoles due to significant interactions between the ligands. In the simulations, both of the MNP rings, formed due to the dipole moments, are oriented as clockwise rotations (**Figure 3** (a), snapshot at 4.0 ns) suggesting that a stable dipolar configuration was not reached even when the total cluster is stable. Hence, this configuration does not attain a complete flux closure, enabling further growth of the cluster due to dipolar interaction alone. Moreover, this final dipolar configuration is sensitive to the initial distance between the dipole moments and their relative orientations.

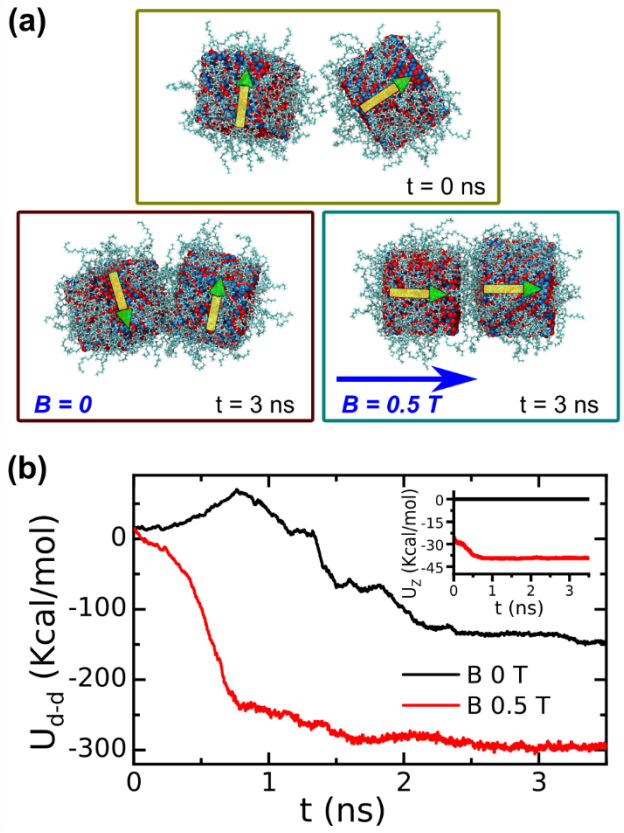

Figure 4. Self-assembly of two cubic Fe_3O_4 nanoparticles in hexane. (a) Top snapshot is the initial simulation set-up at t = 0 (after energy minimization and equilibration), while the bottom snapshots are systems at t = 3 ns without (B = 0) and with (B = 0.5 T) the presence of an external magnetic field. The blue arrow denotes the direction of the applied field. Solvent molecules are hidden for clarity. The scaling factors are $\alpha = 10\ and\ \beta = 16.83$. (b) Dipolar and Zeeman energy (inset) evolution of the two nanocubes without and with the presence of an external magnetic field.

Dipolar Assembly of Cubic Nanoparticles in an External Field

Externally applied magnetic fields can drastically change the morphology and phase behavior of MNP structures by forming linear chains or columns of spherical MNPs parallel to the magnetic field.[77] The assembly of oleic acid-coated cubic Fe_3O_4 MNPs in toluene was previously

investigated by Taheri *et al.*, where the presence of a magnetic field and the existence of a size limit were highlighted.[18] For example, in the presence of an external magnetic field, only nanocubes of size larger than 7.5 nm assembled into structures, which indicates that below this size limit, the dipole moments in the cubes are not strong enough to induce a Brownian rotation of the particles. With the application of the magnetic field, the 1D assembly of the cubic particles was observed in solution. To examine the dynamics of multiple MNPs under the influence of an external field, we similarly employed a simulation system containing two 3.2-nm cubic oleic acid-coated Fe_3O_4 nanoparticles solvated in hexane (**Figure 4** (a)). Here, we initially set up the nanoparticles 75 Å away from each other in the *perpendicular* configuration (**Figure 1** (d)) to avoid any initial preferred interaction. In the absence of an external magnetic field (B = 0), the particles quickly assemble into the favorable *anti-parallel* dipolar configuration. We observed that the assembly remained stable in this configuration due to the strong interaction between the oleic acid ligands, while the dipolar interaction energy decays by r^{-3}. On the other hand, when an external uniform magnetic field is applied (B = 0.5 T), the particles initially undertook a Zeeman rotation similar to the bare MNPs in hexane discussed before, followed by the formation of a stable and aligned 1D assembly in the most favorable *head-to-tail* configuration.

Figure 4 (b) shows the dipole-dipole interaction energy evolution between the two cubic nanoparticles. In the absence of the external magnetic field (B = 0), the self-assembly between the particles is promoted by the ligand-ligand interactions. During the assembly process, the dipole-dipole energy increases by about 50 kcal/mol. Once the self-assembly takes place, the U_{d-d} value starts to decrease as the dipole moments preferentially orient themselves in the *anti-parallel* dipolar configuration. We notice that because of the high values of the scaling factors $\alpha = 10$ and $\beta = 16.83$ used in this simulation, the interaction energy value of -150 kcal/mol is

already strong enough to prevent further rotation of the particles due to thermal fluctuation. As a result, the energy landscape of the assembled structure acts as a local minimum, and the *head-to-tail* configuration, which requires further rotation of the cubes, is never reached. The inset graph shows zero Zeeman energy values due to the absence of the magnetic field. However, when the external magnetic field is applied (B = 0.5 T), the Zeeman energy decreases by 7 kcal/mol as the nanoparticles align themselves with the field. They then self-assemble in the *head-to-tail* configuration. The corresponding global minimum of the dipolar energy landscape of the two-NP system can be assigned as U_{d-d} = -300 kcal/mol. **Figure S6** shows the mass density and the radial distribution function of the hexane molecules around the self-assembled MNPs. The ligand molecules favorably interact with the hexane molecules and the configuration remains stable. Overall, the interplay of Zeeman interaction due to an external field and the favorable interaction between the surfactants of the MNPs will determine the outcome of the assembly.

Formation of Dipolar Ring and Dipolar Chain

Previous theoretical studies on nanoparticle dipole-dipole interactions suggest that the magnetic nanoparticles can form a ring-like structure in the absence of an external field.[43,78] Experimentally, dipole-dipole interaction-mediated nanorings have also been observed for 10-nm to 50-nm Fe_3O_4 MNPs with the size of the formed ring ranging from 100 nm to 1 μm in diameter and in 10-nm Ni-coated Au nanorods with a ring diameter of 250 nm.[79–81] To simulate the ring formation as a means of validation of our method, we placed eight bare MNPs inside the simulation box in vacuum. The initial configuration of this system at 0 ns can be seen in **Figure 5** (a).

The formation of a dipolar ring is dependent on strong dipole-dipole interactions. For example, in the case of rings formed by 47.1-nm Fe_3O_4 MNPs cultured from *magnetotactic bacteria*, the

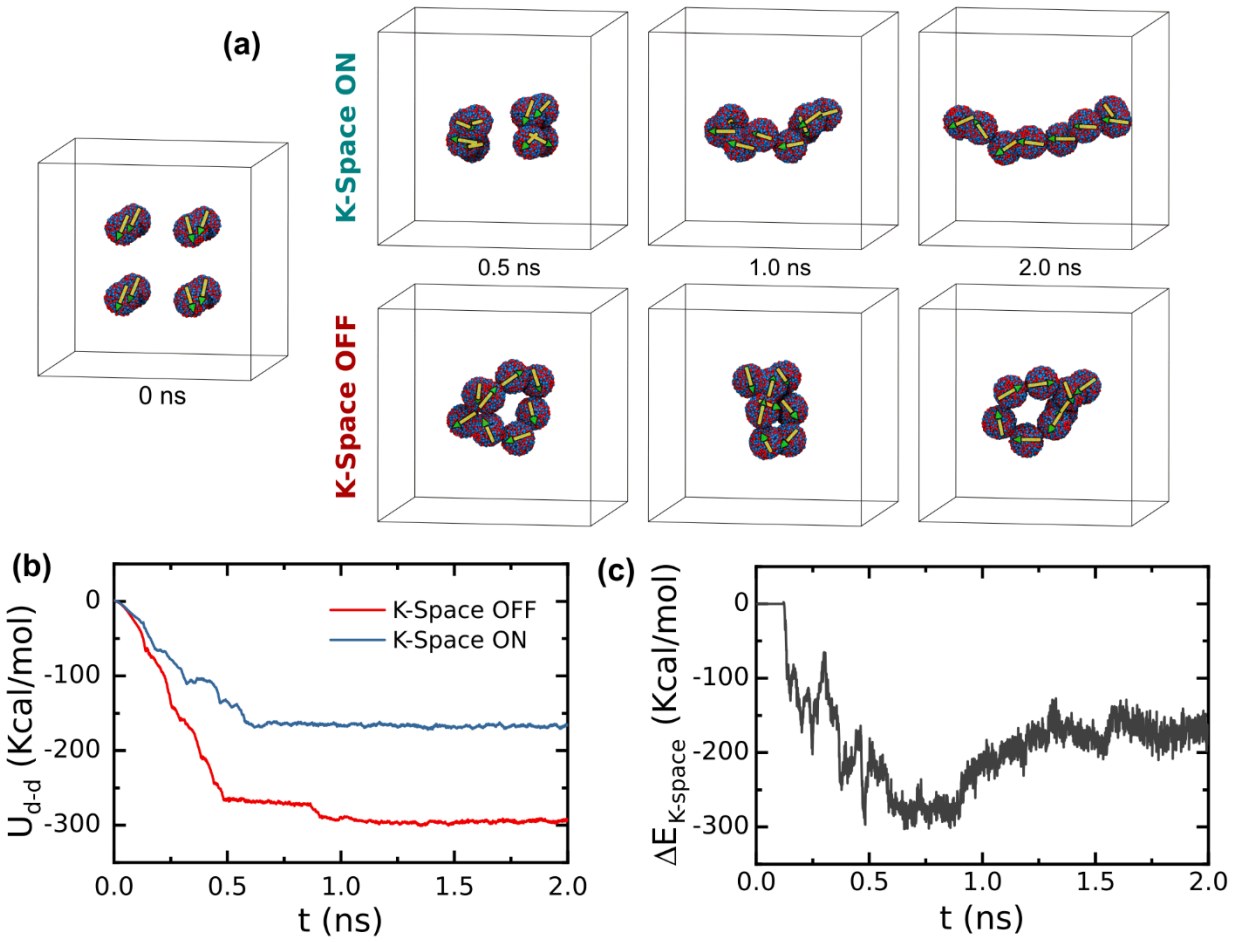

Figure 5. (a) Snapshots of eight bare MNPs simulated in vacuum with and without the long-range electrostatic interaction calculation (implemented as *K-space* solver in LAMMPS) producing ring and chain-like equilibrium structures ($\alpha = 80, \beta = 4$). No external magnetic field was applied. (b) Dipolar energy evolution within the particles. (c) Difference between the system electrostatic energy when the long-range calculation is on and off.

maximum dipolar interaction energy corresponding to the *head-to-tail* configuration has been reported to be around 70 times stronger than thermal energy.[79] We found that the favorable ring formation happens not only in the case of strong dipole-dipole interaction ($\alpha = 80$) but also in the absence of any long-range electrostatic interactions. In our model, the long-range electrostatic interaction is calculated in *K-space* in LAMMPS. Two cases of simulations, with and without the *K-space* calculation (*i.e.*, long-range electrostatics), are shown in the snapshots

in **Figure 5** (a). In both cases, the bare MNPs got closer to each other until 0.5 ns. By 1.0 ns, the *K-space* interaction caused the particles to spread out towards the side of the simulation box to interact with the neighboring periodic boundary condition (PBC) images. On the other hand, when the long-range electrostatic interaction was turned off, the particles continued to form a symmetric ring-like structure. At 2.0 ns, six out of eight MNPs created a circular ring, while the other two MNPs stayed attached to the ring on the side. The long-range electrostatic interaction calculated in *K-space,* however, caused the MNPs to form a long chain-like structure spread throughout the length of the PBC box.

To understand the ring and chain formation energetics, we plotted the dipolar interaction energy values of the eight MNPs in **Figure 5** (b). In both cases, in the absence of any solvent, the MNPs quickly assemble around 0.5 ns. The electrostatic energy values of the two systems differ depending on the method of calculation, for example, when the *K-space* calculation is used, the total electrostatic energy of the system is lower due to long-range contributions. The difference between the total electrostatic energies of the two systems, therefore, defines the contribution due to the long-range electrostatics alone (**Figure 5** (c)). The plot quantifies the energy lost by the system due to long-range electrostatic interaction, which is gained by the dipolar interaction (**Figure 5** (b)), that ultimately promotes the formation of the line across the periodic box. Theoretical calculations suggest that a ring of eight magnetic spheres is more energetically favorable than a line.[39] The energy, U_{d-d}, graphs also agree with such a prediction. However, our results indicate that, at the nanoscale, long-range electrostatic interaction may promote line formation instead of ring formation.

Advantages and Limitations of the Modeling Method

The primary advantage of our model is the atomistic resolution of the MNP core, surfactants, and the solvents. Various surface energies of the core, for example, MNPs carrying a net surface charge, having a specific functionalization, can be simulated without assuming any approximate treatment of the material. MNPs with ligands of any size, chemistry, branching, functionalization, *etc*. can be modeled along with the MNP core, and the corresponding dynamics, packing, and interaction with solvent molecules can be captured with the model. While the long-range hydrodynamic effects are automatically captured by the simulated all-atom solvent molecules, other effects of viscosity, the presence of interfaces and ions, and various pH conditions can also be studied to better represent MNPs in various *in-situ* and *in-vivo* conditions. In addition, since the rigid-body model of the core works by summing up the individual atomic interactions, no additional force field parameterization is required, and existing atomistic force fields can be used in the model. The rigid-body model has an even more significant advantage that MNP cores with any arbitrary shapes and sizes can be easily constructed without sacrificing the atomistic details. While we have shown here the use of spherical and cubic MNPs, additional shapes such as an ellipsoid, rod, lobe, etc. with different sizes can be used in the model. Furthermore, the relative distance between the atoms of the rigid core is kept fixed, which provides added benefits such as the ability to turn off intra-body interactions to save time in computations.[67] Another major advantage of the model is the ability to define and tune the strength and orientation of the magnetic dipole moments of the modeled MNP(s) using Equation (1) and the scaling factor, β. For example, anisotropic MNPs, such as cubes, have inherent magnetic anisotropy where the easy axis of the dipole moment can orient towards the [111] or [001] direction depending on the material. An example of a [001] axis-oriented cubic MNP has

been presented in our work; however, any other directions can be specified for the dipole by choosing an appropriate pair of head and tail *Ms* atoms inside the MNP core. Moreover, by selecting multiple pairs of atoms in the LAMMPS input file, more than one dipole moment can be readily defined in the MNP core to capture the dynamics of a multidomain MNP. Likewise, the ability to simulate the influences of an external magnetic field is necessary to study a wide range of applications of MNPs in targeted drug delivery, hyperthermia, sensing and magnetic imaging. Atomic and molecular-level phenomena, such as the interplay of the solvent and ligands with the Zeeman force applied by the external field can be examined using the proposed model as long as the applied magnetic field remains time-invariant. Lastly, we have developed the plugin to make use of multiple CPU cores using MPI parallelization typically available in a modern computer. Therefore, for large MNP systems, the simulation model can be efficiently used in a high-performance computing facility. For example, in the system of two nanocubes solvated in explicit hexane solvent with a total number of 203,436 atoms, where both dipolar interactions and external field interactions were calculated, a speed of 1.14 ns/day was obtained using 6 Intel Xeon E5-2630 v3 (2.40 GHz) MPI cores and 2 NVIDIA GeForce GTX Titan X (12 GB, 250 W) GPU cards. However, it is worth noting that, 18.15% and 56.68% CPU computation time were spent on long range electrostatic calculations and bond energy calculations respectively, while only 7.78% of the CPU computation time was spent on the magnetic interaction calculation algorithm. Thus, the model proposed here does not significantly affect the simulation speed.

While the proposed model allows us to study the magnetically induced nanoscale phenomena with full atomic-level resolution, owing to computational limitations and to keep the method simple, some restrictions were assumed. First, a typical 3.2-nm Fe_3O_4 MNP does not have a

strong magnetic dipole moment to generate Brownian rotation induced by the magnetic field.[18] To overcome this challenge, we scaled up the dipole moments by the scaling factor β. With more computational resources available and for simulations of a large MNP with size above 7 nm, this scaling factor can be set to unity thereby eliminating the need for this approximation. Also, the dipole-dipole scaling factor, α was set according to the suggestions provided by the previous studies.[56,57,79,82] Additionally, an MNP with a size below 12 nm may experience Neel rotation in an external field[17] which was ignored in the simulation by assuming a magnetically hard MNP. Second, to maintain a conservative simulation system, the externally applied magnetic field was assumed to be time-independent. Though our current work focuses on a uniform magnetic field, the model can still be used to simulate the nanoparticle dynamics in a static non-uniform magnetic field. The Lorentz force effects were ignored for the same reason, which would require the introduction of a new integration algorithm that can maintain system ergodicity. Plasmonic 80-nm gold nanoparticles illuminated by a strong laser beam have been reported to form long chains due to mutual Lorentz forces experienced by the electric dipole moments of the particles.[83] However, for the magnetic NPs the Lorentz force effect leads to an increased diffusion of the particles in a direction orthogonal to the applied magnetic field.[84] Since the direction of a magnetic dipole moment does not affect the Lorentz force direction, we can similarly expect an accelerated diffusion of the MNPs in a direction perpendicular to the velocity of the MNPs and the direction of the applied magnetic field. Moreover, depending on the direction of the motion of individual particles, Lorentz force may accelerate or retard assembly formation between the MNPs. Finally, unlike the long-range hydrodynamic or electrostatic interactions, the dipolar interactions produced by the weak dipole moments of a typical nanoparticle with a size below 30 nm becomes negligible. Hence, in our current implementation,

the d-d interaction between multiple MNPs is calculated by a simple pair-wise summation with a cutoff of 10 times the diameter of the particles. Owing to the rapid decay of the dipolar interactions, such a cutoff has been reported to create a negligible but non-zero error of $0.05\ K_BT$.[46] In a system where a large number of MNPs are present, a better implementation of the dipolar interactions would require a many-body interactions calculation method, such as the Ewald summation method.[85] Moreover, a shifted dipole-dipole interaction potential would make the calculation more exact. We acknowledge these limitations of the current work and leave the needed improvements for future studies. We note that the described limitations do not affect the results reported in the preceding sections about the solvent and ligand interactions, long-range electrostatic interactions, shape effects and short-range effects of the dipolar interactions.

CONCLUSIONS

In summary, we presented a novel all-atom MD simulation method to model the dipolar interactions and external magnetic field-induced Zeeman interactions of single-domain, magnetically hard nanoparticles. Our study revealed novel phenomena related to the effects of oleic acid ligands, polar solvents, and long-range electrostatic interactions on the magnetic particles. The results indicate that for smaller nanoparticles, solvent polarity and the long-range Coulombic interactions influence MNP diffusion. Dipole-mediated self-assembly simulations indicated that the dipolar interaction creates clusters with high order and symmetry, while the interplay between ligands due to VDW interactions enable the cluster to grow in size. The mechanism of line formation by cubic nanoparticles reported in the past experimental studies is elucidated, demonstrating the role of the external magnetic field on the formation of ordered 1D lines in a solvent environment. Finally, dipolar-ring and line formations are found to be highly sensitive to the strength of the dipole moment. While the ring formation is theoretically

favorable, a 1D line can form due to long-range electrostatic interactions; this effect may depend on MNP concentrations, solvent and the initial configuration. Therefore, undesired artifacts may arise if the long-range electrostatic interactions are ignored in the study of MNP systems, particularly for those where the MNPs carry a net surface charge. We anticipate that our method can be used to study the interactions between magnetic nanoparticles with a high resolution, which can further be used to determine the interaction potentials used in coarse-grained simulation techniques. The source code of the model is published in a publicly available GitHub repository as a LAMMPS software plugin for reusability.[86]

METHOD

Magnetic Nanoparticle Model Construction

Superparamagnetic iron oxide Fe_3O_4 nanoparticles were considered for our model MNP in this study. Bulk Fe_3O_4 has an inverse spinel structure with an Fd-3m space group containing both Fe_2^+ and Fe_3^+ atoms. A CIF file (COD ID 9007644) containing the Fe_3O_4 crystal structure was downloaded from the Crystallography Open Database.[87] Using the Mercury 3.9 software, the unit cell of the Fe_3O_4 structure was constructed from the CIF file.[88] The unit cell was translated in three dimensions to build the cubic nanoparticle of 3.2-nm size using the *leap* program of the AmberTools 18 software package.[89] For the spherical core model, a larger 5-nm cubic cell was first built, and then a sphere was cut out by selecting the atoms within a 16-Å radius from the center of the cube mass. Covalent bonds were assigned within a 2.1-Å cutoff distance between the atoms of the cubic cells using the *leap* program. The undercoordinated atoms from the surface of the sphere were deleted. The resulting spherical core carried 1,622 atoms (924 O; 468 octahedral Fe; 230 tetrahedral Fe), and the cubic core carried 3,580 atoms (2,048 O; 1,024 octahedral Fe; 508 tetrahedral Fe). In an aqueous system, freshly prepared magnetite

nanoparticles were reported to carry a net positive surface charge density at neutral pH.[90] Hence, a second bare spherical core having a net positive surface charge density of +0.05 C/m^2 was constructed to study the effect of the surface charge on particle alignment. To add the net surface charge, the MNP atoms were divided into "surface atoms", by selecting a 2-Å shell of surface atoms, and "bulk atoms", the remaining atoms within the center of the MNP. The partial charges of the "surface atoms" were then adjusted to yield a net +0.05 C/m^2 value. The partial charges of the "bulk atoms" were then adjusted to counterbalance this additional charge on the surface, making the whole nanoparticle core charge neutral. A schematic showing the method of surface atom selection and corresponding atomic partial charges is shown in **Figure S7**. The non-bonded parameters of the force field for the Fe and O atoms were taken from the Universal Force Field (UFF) by Rappe *et al.*[91] All the atoms within the rigid core moved as a single entity, thereby eliminating the need for the bonded terms in the force field. To create a dipole moment vector, two atoms were selected along the opposite ends of an arbitrary diameter vector in the core. The type of these two atoms was set as "Ms", which was later used by the LAMMPS plugin to identify and calculate the dipole moment vector during the simulation.

For ligand functionalization of MNPs, the experimental oleic acid densities on spherical Fe_3O_4 MNPs lie between 2.5-3.0 nm^{-2}.[92] In our model, we covalently attached 90 oleic acid ligands onto the charge-neutral spherical core and 76 oleic acid ligands onto the cubic core yielding a grafting density of 2.79 nm^{-2} and 1.86 nm^{-2}, respectively. During the attachment process, both O atoms of the deprotonated carboxyl group of the oleic acid were covalently linked to a single surface Fe_3^+ atom (bi-dented bonding) for simplicity. The partial charges of the oleic acid and the solvent molecules were calculated with the General Atomic and Molecular Electronic Structure System (GAMESS) 5DEC14R1 package[93] by fitting the electrostatic potential surface using the

default Restrained Electrostatic Potential (RESP-A1) charge model[94] implemented in the R.E.D. Tools III.[95] The other bonded and non-bonded terms of the force field for the oleic acid and the solvent molecules were parameterized using GAFF2.[96] The calculated partial charges of the molecules and force field parameters are detailed in **Figure S8** and **Table S2, S3**. The dipole moment of the MNP was calculated by assuming a fully saturated MNP and multiplying the volume of the MNP core with the bulk saturation magnetization value of 480 kA/m for Fe_3O_4 nanoparticles.[44] The constructed final MNP structures are shown in **Figure 1** (a).

MD Simulation Setup

All-atom MD simulations were conducted using the LAMMPS[97] simulation software. The 'lj/cut/coul/long' *pair_style* was used to calculate the pairwise interactions with an 8.0-Å cutoff. Unless otherwise specified, a 15.0-Å buffer was used between the solute MNPs and the periodic boundaries of the simulation box. The calculated average density value for an ethanol solvent box was 0.7726 ± 0.0098 g/cm^3 and for a hexane solvent box was 0.6622 ± 0.0081 g/cm^3 at 300 K and 1 atm. The Particle-Particle Particle-Mesh (PPPM)[98] type *K-space* solver with a precision value of 1.0E-4 was used to calculate the long-range Coulombic interactions. All systems were initially energy minimized for 500 energy iterations and 1,000 force evaluations using the conjugate gradient algorithm to remove any overlap between the atoms. They were then heated from 0 to 300 K for 90 ps, followed by a 200-ps NVT equilibration at 300 K. A subsequent NPT equilibration for 1 ns was conducted at 300 K and 1 atm. All production simulations were finally conducted in NVT conditions. A time step of 1 fs was used throughout the simulation. The Nosé-Hoover thermostat with a damping constant of 0.01 ps was implemented for temperature control during the NVT production simulations.[99] Periodic boundary conditions (PBCs) were implemented in all three directions. The developed rigid-body dynamics-based plugin, *MSPIN*,

was used only during the production simulation to input the information of the dipole moments, external magnetic field, and to calculate the magnetic interactions between the MNP cores. Rotations of the bare MNPs were simulated for 5 ns. The assembly of eight MNPs was simulated for 20 ns, and the assembly of cubic MNPs was simulated for 4 ns. The simulation of ring and line formation was conducted for 5 ns. While we typically employ longer simulation times (50 ns to 1 μs) for modeling equilibrium properties of materials,[100–103] and the choice of time depends on the size and complexity of the system, simulation results presented here are for non-equilibrium conditions, which warrants shorter simulation times. A summary of the simulated systems including system size, solvent numbers, runtime, *etc*. is provided in **Table S1**.

All visualizations were performed using the Visual Molecular Dynamics software.[104] The magnetic dipolar and Zeeman interaction energies were calculated with the developed MSPIN plugin using Equations (2) and (3). The total system energies were reported by the LAMMPS software during the simulations, and the VDW interaction energy between the MNP surfactants was calculated using the *lie* command of the CPPTraj analysis software.[105]

Abbreviations

MNP, Magnetic Nanoparticle; MD, Molecular Dynamics; d-d, Dipole-Dipole; MC, Monte Carlo; CG, Coarse Grained; LD, Langevin Dynamics; VDW, van der Waals; PBC, Periodic Boundary Conditions.

ACKNOWLEDGEMENT

The authors would like to thank Prof. J. B. Tracy and M. H. Rizvi for their helpful comments and suggestions during the course of this work, and Prof. A. L. Kwansa for his inputs and

administration of the GPU servers used to perform these simulations. This research was funded by the National Science Foundation (grant number CMMI-1763025).

SUPPORTING INFORMATION

The supporting information is available free of charge via the Internet at http://pubs.acs.org

- Additional details about simulation protocol, analyses, data, and the source code of the developed LAMMPS plugin. (PDF)
- Movie 1: Zeeman rotation of a bare spherical MNP in hexane (MPG)
- Movie 2: Dipolar assembly of eight spherical MNPs in vacuum (MPG)
- Movie 3: Dipolar assembly of two cubic MNPs in hexane (MPG)
- Movie 4: Formation of dipolar ring by eight spherical MNPs (MPG)

AUTHOR INFORMATION

Corresponding Author

Yaroslava G. Yingling − Department of Materials Science and Engineering, North Carolina State University, Raleigh, North Carolina 27695, United States; https://orcid.org/0000-0002-8557-9992; E-mail: yara_yingling@ncsu.edu

Authors

Akhlak U. Mahmood − Department of Materials Science and Engineering, North Carolina State University, Raleigh, North Carolina 27695, United States; https://orcid.org/0000-0002-5607-2885

Author Contributions

The manuscript was written through contributions of all authors. All authors have given approval to the final version of the manuscript.

Conflict of Interest

The authors declare no competing financial interest.

REFERENCES

(1) Billas, I. M. L.; Châtelain, A.; de Heer, W. A. Magnetism from the Atom to the Bulk in Iron, Cobalt, and Nickel Clusters. *Science* **1994**, *265* (5179), 1682–1684.

(2) Chang, Y.; Shi, J.; Tang, Y.; Zhang, H.; Yue, Z.; Yao, W.; Bai, Y.; Cao, J. Investigation of Significant Magnetic Transformation for Hydrogenated ZnFe2O4 Nanoparticles. *J. Mater. Sci.* **2020**, *55* (4), 1464–1474.

(3) Scholten, P. C.; Tjaden, D. L. A. Mutual Attraction of Superparamagnetic Particles. *J. Colloid Interface Sci.* **1980**, *73* (1), 254–255.

(4) Reiss, G.; Hütten, A. Magnetic Nanoparticles Applications Beyond Data Storage. *Nat. Mater.* **2005**, *4* (10), 725–726.

(5) Hua, M. Y.; Yang, H. W.; Liu, H. L.; Tsai, R. Y.; Pang, S. T.; Chuang, K. L.; Chang, Y. S.; Hwang, T. L.; Chang, Y. H.; Chuang, H. C.; Chuang, C. K. Superhigh-Magnetization Nanocarrier as a Doxorubicin Delivery Platform for Magnetic Targeting Therapy. *Biomaterials* **2011**, *32* (34), 8999–9010.

(6) Shapiro, B.; Kulkarni, S.; Nacev, A.; Muro, S.; Stepanov, P. Y.; Weinberg, I. N. Open Challenges in Magnetic Drug Targeting. *Wiley Interdiscip. Rev. Nanomed. Nanobiotechnol.* **2015**, *7* (3), 446–457.

(7) Arias, L. S.; Pessan, J. P.; Vieira, A. P. M.; de Lima, T. M. T.; Delbem, A. C. B.; Monteiro, D. R. Iron Oxide Nanoparticles for Biomedical Applications: A Perspective on Synthesis, Drugs, Antimicrobial Activity, and Toxicity. *Antibiotics* **2018**, *7* (2), No. 46.

(8) Bao, Y.; Wen, T.; Samia, A. C. S.; Khandhar, A.; Krishnan, K. M. Magnetic Nanoparticles: Material Engineering and Emerging Applications in Lithography and Biomedicine. *J. Mater. Sci.* **2016**, *51* (1), 513–553.

(9) Chen, W. D.; Kohll, A. X.; Nguyen, B. H.; Koch, J.; Heckel, R.; Stark, W. J.; Ceze, L.; Strauss, K.; Grass, R. N. Combining Data Longevity with High Storage Capacity—Layer-by-Layer DNA Encapsulated in Magnetic Nanoparticles. *Adv. Funct. Mater.* **2019**, *29* (28), No. 1901672.

(10) Schmauch, M. M.; Mishra, S. R.; Evans, B. A.; Velev, O. D.; Tracy, J. B. Chained Iron Microparticles for Directionally Controlled Actuation of Soft Robots. *ACS Appl. Mater. Interfaces* **2017**, *9* (13), 11895–11901.

(11) Bennet, M.; Bertinetti, L.; K. Neely, R.; Schertel, A.; Körnig, A.; Flors, C.; D. Müller, F.; Schüler, D.; Klumpp, S.; Faivre, D. Biologically Controlled Synthesis and Assembly of Magnetite Nanoparticles. *Faraday Discuss.* **2015**, *181* (0), 71–83.

(12) Thomas, J. R. Preparation and Magnetic Properties of Colloidal Cobalt Particles. *J. Appl. Phys.* **1966**, *37* (7), 2914–2915.

(13) Wang, H.; Brandl, D. W.; Le, F.; Nordlander, P.; Halas, N. J. Nanorice: A Hybrid Plasmonic Nanostructure. *Nano Lett.* **2006**, *6* (4), 827–832.

(14) Wetterskog, E.; Agthe, M.; Mayence, A.; Grins, J.; Wang, D.; Rana, S.; Ahniyaz, A.; Salazar-Alvarez, G.; Bergström, L. Precise Control Over Shape and Size of Iron Oxide Nanocrystals Suitable for Assembly into Ordered Particle Arrays. *Sci. Technol. Adv. Mater.* **2014**, *15* (5), No. 055010.

(15) Goya, G. F.; Berquó, T. S.; Fonseca, F. C.; Morales, M. P. Static and Dynamic Magnetic Properties of Spherical Magnetite Nanoparticles. *J. Appl. Phys.* **2003**, *94* (5), 3520–3528.

(16) Rossi, L.; Donaldson, J. G.; Meijer, J.-M.; Petukhov, A. V; Kleckner, D.; Kantorovich, S. S.; Irvine, W. T. M.; Philipse, A. P.; Sacanna, S. Self-Organization in Dipolar Cube Fluids Constrained by Competing Anisotropies. *Soft Matter* **2018**, *14* (7), 1080–1087.

(17) Erné, B. H.; Butter, K.; Kuipers, B. W. M.; Vroege, G. J. Rotational Diffusion in Iron Ferrofluids. *Langmuir* **2003**, *19* (20), 8218–8225.

(18) Taheri, S. M.; Michaelis, M.; Friedrich, T.; Förster, B.; Drechsler, M.; Römer, F. M.; Bösecke, P.; Narayanan, T.; Weber, B.; Rehberg, I.; Rosenfeldt, S.; Förster, S. Self-Assembly of Smallest Magnetic Particles. *Proc. Natl. Acad. Sci. USA* **2015**, *112* (47), 14484–14489.

(19) Rosenfeldt, S.; Förster, S.; Friedrich, T.; Rehberg, I.; Weber, B. Self-Assembly of Magnetic Iron Oxide Nanoparticles into Cuboidal Superstructures. In *Novel Magnetic Nanostructures*; Domracheva, N., Caporali, M., Rentschler, E., Eds.; Advanced Nanomaterials; Elsevier, 2018; pp 165–189.

(20) Singh, G.; Chan, H.; Baskin, A.; Gelman, E.; Repnin, N.; Král, P.; Klajn, R. Self-Assembly of Magnetite Nanocubes into Helical Superstructures. *Science* **2014**, *345* (6201), 1149–1153.

(21) Ahniyaz, A.; Sakamoto, Y.; Bergström, L. Magnetic Field-Induced Assembly of Oriented Superlattices from Maghemite Nanocubes. *Proc. Natl. Acad. Sci. USA* **2007**, *104* (45), 17570–17574.

(22) Stanković, I.; Lizardi, L.; García, C. Assembly of Nanocube Super-Structures Directed by Surface and Magnetic Interactions. *Nanoscale* **2020**, *12* (37), 19390–19403.

(23) Pyanzina, E. S.; Gudkova, A. V; Donaldson, J. G.; Kantorovich, S. S. Cluster Analysis in Systems of Magnetic Spheres and Cubes. *J. Magn. Magn. Mater.* **2017**, *431*, 201–204.

(24) Cheng, G.; Romero, D.; Fraser, G. T.; Hight Walker, A. R. Magnetic-Field-Induced Assemblies of Cobalt Nanoparticles. *Langmuir* **2005**, *21* (26), 12055–12059.

(25) Bharti, B.; Kogler, F.; Hall, C. K.; Klapp, S. H. L.; Velev, O. D. Multidirectional Colloidal Assembly in Concurrent Electric and Magnetic Fields. *Soft Matter* **2016**, *12* (37), 7747–7758.

(26) Maldonado-Camargo, L.; Yang, C.; Rinaldi, C. Scale-Dependent Rotational Diffusion of Nanoparticles in Polymer Solutions. *Nanoscale* **2017**, *9* (33), 12039–12050.

(27) Li, Z. Critical Particle Size Where the Stokes-Einstein Relation Breaks Down. *Phys. Rev. E* **2009**, *80* (6), No. 61204.

(28) Kharazmi, A.; Priezjev, N. V. Diffusion of a Janus Nanoparticle in an Explicit Solvent: A Molecular Dynamics Simulation Study. *J. Chem. Phys.* **2015**, *142* (23), No. 234503.

(29) Heyes, D. M.; Nuevo, M. J.; Morales, J. J.; Branka, A. C. Translational and Rotational Diffusion of Model Nanocolloidal Dispersions Studied by Molecular Dynamics Simulations. *J. Phys.: Condens. Matter* **1998**, *10* (45), 10159–10178.

(30) Bian, B.; Chen, G.; Zheng, Q.; Du, J.; Lu, H.; Liu, J. P.; Hu, Y.; Zhang, Z. Self-Assembly of CoPt Magnetic Nanoparticle Arrays and Its Underlying Forces. *Small* **2018**, *14* (34), No. 1801184.

(31) Dijkstra, M.; Luijten, E. From Predictive Modelling to Machine Learning and Reverse Engineering of Colloidal Self-Assembly. *Nat. Mater.* **2021**, *20* (6), 762–773.

(32) Boyen, H.-G.; Fauth, K.; Stahl, B.; Ziemann, P.; Kästle, G.; Weigl, F.; Banhart, F.; Hessler, M.; Schütz, G.; Gajbhiye, N. S.; Ellrich, J.; Hahn, H.; Büttner, M.; Garnier, M. G.; Oelhafen, P. Electronic and Magnetic Properties of Ligand-Free FePt Nanoparticles. *Adv. Mater.* **2005**, *17* (5), 574–578.

(33) Jin, Y.; Jia, C.; Huang, S.-W.; O'Donnell, M.; Gao, X. Multifunctional Nanoparticles as Coupled Contrast Agents. *Nat. Commun.* **2010**, *1* (1), No. 41.

(34) Goon, I. Y.; Lai, L. M. H.; Lim, M.; Munroe, P.; Gooding, J. J.; Amal, R. Fabrication and Dispersion of Gold-Shell-Protected Magnetite Nanoparticles: Systematic Control Using Polyethyleneimine. *Chem. Mater.* **2009**, *21* (4), 673–681.

(35) Vasilakaki, M.; Ntallis, N.; Yaacoub, N.; Muscas, G.; Peddis, D.; N. Trohidou, K. Optimising the Magnetic Performance of Co Ferrite Nanoparticles Via Organic Ligand Capping. *Nanoscale* **2018**, *10* (45), 21244–21253.

(36) Huaman, J. L. C.; Fukao, S.; Shinoda, K.; Jeyadevan, B. Novel Standing Ni–Pt Alloy Nanocubes. *CrystEngComm* **2011**, *13* (10), 3364–3369.

(37) Gul, S.; Khan, S. B.; Rehman, I. U.; Khan, M. A.; Khan, M. I. A Comprehensive Review of Magnetic Nanomaterials Modern Day Theranostics. *Front. Mater.* **2019**, *6*, No. 179.

(38) van Leeuwen, D. A.; van Ruitenbeek, J. M.; de Jongh, L. J.; Ceriotti, A.; Pacchioni, G.; Häberlen, O. D.; Rösch, N. Quenching of Magnetic Moments by Ligand-Metal Interactions in Nanosized Magnetic Metal Clusters. *Phys. Rev. Lett.* **1994**, *73* (10), 1432–1435.

(39) Abelmann, L.; Hageman, T. A. G.; Löthman, P. A.; Mastrangeli, M.; Elwenspoek, M. C. Three-Dimensional Self-Assembly Using Dipolar Interaction. *Sci. Adv.* **2020**, *6* (19), No. eaba2007.

(40) Faure, B.; Wetterskog, E.; Gunnarsson, K.; Josten, E.; P. Hermann, R.; Brückel, T.; Wenzel Andreasen, J.; Meneau, F.; Meyer, M.; Lyubartsev, A.; Bergström, L.; Salazar-Alvarez, G.; Svedlindh, P. 2D to 3D Crossover of the Magnetic Properties in Ordered Arrays of Iron Oxide Nanocrystals. *Nanoscale* **2013**, *5* (3), 953–960.

(41) Zablotsky, D.; Rusevich, L. L.; Zvejnieks, G.; Kuzovkov, V.; Kotomin, E. Manifestation of Dipole-Induced Disorder in Self-Assembly of Ferroelectric and Ferromagnetic Nanocubes. *Nanoscale* **2019**, *11* (15), 7293–7303.

(42) Klapp, S. H. L. Collective Dynamics of Dipolar and Multipolar Colloids: From Passive to Active Systems. *Curr. Opin. Colloid Interface Sci.* **2016**, *21*, 76–85.

(43) Jacobs, I. S.; Bean, C. P. An Approach to Elongated Fine-Particle Magnets. *Phys. Rev.* **1955**, *100* (4), 1060–1067.

(44) Butter, K.; Bomans, P. H.; Frederik, P. M.; Vroege, G. J.; Philipse, A. P. Direct Observation of Dipolar Chains in Ferrofluids in Zero Field Using Cryogenic Electron Microscopy. *J. Phys.: Condens. Matter* **2003**, *15* (15), S1451–S1470.

(45) Weis, J. J. Orientational Structure of Quasi-Two-Dimensional Dipolar Hard Spheres. *Mol. Phys.* **1998**, *93* (3), 361–364.

(46) Andreu, J. S.; Camacho, J.; Faraudo, J. Aggregation of Superparamagnetic Colloids in Magnetic Fields: The Quest for the Equilibrium State. *Soft Matter* **2011**, *7* (6), No. 2336.

(47) Ku, J.; Aruguete, D. M.; Alivisatos, A. P.; Geissler, P. L. Self-Assembly of Magnetic Nanoparticles in Evaporating Solution. *J. Am. Chem. Soc.* **2011**, *133* (4), 838–848.

(48) Them, K. On Magnetic Dipole–Dipole Interactions of Nanoparticles in Magnetic Particle Imaging. *Phys. Med. Biol.* **2017**, *62* (14), 5623–5639.

(49) Ye, H.; Shen, Z.; Li, Y. Computational Modeling of Magnetic Particle Margination within Blood Flow through LAMMPS. *Comput. Mech.* **2018**, *62* (3), 457–476.

(50) Zhang, X.; Zhang, Z.; Glotzer, S. C. Simulation Study of Dipole-Induced Self-Assembly of Nanocubes. *J. Phys. Chem. C* **2007**, *111* (11), 4132–4137.

(51) John, B. S.; Stroock, A.; Escobedo, F. A. Cubatic Liquid-Crystalline Behavior in a System of Hard Cuboids. *J. Chem. Phys.* **2004**, *120* (19), 9383–9389.

(52) Donaldson, J. G.; Kantorovich, S. S. Directional Self-Assembly of Permanently Magnetised Nanocubes in Quasi Two Dimensional Layers. *Nanoscale* **2015**, *7* (7), 3217–3228.

(53) Håkonsen, V.; Singh, G.; Normile, P. S.; De Toro, J. A.; Wahlström, E.; He, J.; Zhang, Z. Magnetically Enhanced Mechanical Stability and Super-Size Effects in Self-Assembled Superstructures of Nanocubes. *Adv. Funct. Mater.* **2019**, *29* (46), No. 1904825.

(54) in 't Veld, P. J.; Plimpton, S. J.; Grest, G. S. Accurate and Efficient Methods for Modeling Colloidal Mixtures in an Explicit Solvent Using Molecular Dynamics. *Comput. Phys. Commun.* **2008**, *179* (5), 320–329.

(55) Khandhar, A. P.; Ferguson, R. M.; Arami, H.; Krishnan, K. M. Monodisperse Magnetite Nanoparticle Tracers for in Vivo Magnetic Particle Imaging. *Biomaterials* **2013**, *34* (15), 3837–3845.

(56) Allia, P.; Tiberto, P. Dynamic Effects of Dipolar Interactions on the Magnetic Behavior of Magnetite Nanoparticles. *J. Nanopart. Res.* **2011**, *13* (12), 7277–7293.

(57) Sánchez, F. H.; Mendoza Zélis, P.; Arciniegas, M. L.; Pasquevich, G. A.; Fernández van Raap, M. B. Dipolar Interaction and Demagnetizing Effects in Magnetic Nanoparticle Dispersions: Introducing the Mean-Field Interacting Superparamagnet Model. *Phys. Rev. B* **2017**, *95* (13), No. 134421.

(58) Politi, P.; Pini, M. G. Dipolar Interaction Between Two-Dimensional Magnetic Particles. *Phys. Rev. B* **2002**, *66* (21), No. 214414.

(59) Toukmaji, A.; Sagui, C.; Board, J.; Darden, T. Efficient Particle-Mesh Ewald Based Approach to Fixed and Induced Dipolar Interactions. *J. Chem. Phys.* **2000**, *113* (24), 10913–10927.

(60) Nash, J. A.; Singh, A.; Li, N. K.; Yingling, Y. G. Characterization of Nucleic Acid Compaction with Histone-Mimic Nanoparticles through All-Atom Molecular Dynamics. *ACS Nano* **2015**, *9* (12), 12374–12382.

(61) Railsback, J. G.; Singh, A.; Pearce, R. C.; McKnight, T. E.; Collazo, R.; Sitar, Z.; Yingling, Y. G.; Melechko, A. V. Weakly Charged Cationic Nanoparticles Induce DNA Bending and Strand Separation. *Adv. Mater.* **2012**, *24* (31), 4261–4265.

(62) Nash, J. A.; Tucker, T. L.; Therriault, W.; Yingling, Y. G. Binding of Single Stranded Nucleic Acids to Cationic Ligand Functionalized Gold Nanoparticles. *Biointerphases* **2016**, *11* (4), No. 04B305.

(63) Ryckaert, J. P.; Ciccotti, G.; Berendsen, H. J. C. Numerical Integration of the Cartesian Equations of Motion of a System with Constraints: Molecular Dynamics of n-Alkanes. *J. Comput. Phys.* **1977**, *23* (3), 327–341.

(64) Andersen, H. C. Rattle: A "Velocity" Version of the Shake Algorithm for Molecular Dynamics Calculations. *J. Comput. Phys.* **1983**, *52* (1), 24–34.

(65) Kamberaj, H.; Low, R. J.; Neal, M. P. Time Reversible and Symplectic Integrators for Molecular Dynamics Simulations of Rigid Molecules. *J. Chem. Phys.* **2005**, *122* (22), No. 224114.

(66) Nguyen, T. D.; Phillips, C. L.; Anderson, J. A.; Glotzer, S. C. Rigid Body Constraints Realized in Massively-Parallel Molecular Dynamics on Graphics Processing Units. *Comput. Phys. Commun.* **2011**, *182* (11), 2307–2313.

(67) Nguyen, T. D.; Plimpton, S. J. Aspherical Particle Models for Molecular Dynamics Simulation. *Comput. Phys. Commun.* **2019**, *243*, 12–24.

(68) Amber 2021 Reference Manual. https://ambermd.org/doc12/Amber21.pdf#page=264 (accessed Feb 3, 2022).

(69) Griffiths, D. J. Introduction to Electrodynamics; Cambridge University Press: Cambridge, 2017.

(70) Channell, P. J.; Scovel, C. Symplectic Integration of Hamiltonian Systems. *Nonlinearity* **1990**, *3* (2), 231–259.

(71) Spreiter, Q.; Walter, M. Classical Molecular Dynamics Simulation with the Velocity Verlet Algorithm at Strong External Magnetic Fields. *J. Comput. Phys.* **1999**, *152* (1), 102–119.

(72) Zhang, Z.-T.; Zhao, X.; Cao, B.-Y. Diffusion Tensors of Arbitrary-Shaped Nanoparticles in Fluid by Molecular Dynamics Simulation. *Sci. Rep.* **2019**, *9* (1), No. 18943.

(73) Schönke, J.; Schneider, T. M.; Rehberg, I. Infinite Geometric Frustration in a Cubic Dipole Cluster. *Phys. Rev. B* **2015**, *91* (2), No. 20410.

(74) Hartung, S.; Sommer, F.; Völkel, S.; Schönke, J.; Rehberg, I. Assembly of Eight Spherical Magnets into a Dotriacontapole Configuration. *Phys. Rev. B* **2018**, *98* (21), No. 214424.

(75) Messina, R.; Khalil, L. A.; Stanković, I. Self-Assembly of Magnetic Balls: From Chains to Tubes. *Phys. Rev. E* **2014**, *89* (1), No. 011202.

(76) Požar, M.; Lovrinčević, B.; Zoranić, L.; Primorać, T.; Sokolić, F.; Perera, A. Micro-Heterogeneity Versus Clustering in Binary Mixtures of Ethanol with Water or Alkanes. *Phys. Chem. Chem. Phys.* **2016**, *18* (34), 23971–23979.

(77) Holm, C.; Weis, J.-J. The Structure of Ferrofluids: A Status Report. *Curr. Opin. Colloid Interface Sci.* **2005**, *10* (3), 133–140.

(78) Messina, R.; Stanković, I. Self-Assembly of Magnetic Spheres in Two Dimensions: The Relevance of Onion-Like Structures. *EPL* **2015**, *110* (4), No. 46003.

(79) Philipse, A. P.; Maas, D. Magnetic Colloids from Magnetotactic Bacteria: Chain Formation and Colloidal Stability. *Langmuir* **2002**, *18* (25), 9977–9984.

(80) Ahmed, W.; Laarman, R. P. B.; Hellenthal, C.; Kooij, E. S.; Silfhout, A. van; Poelsema, B. Dipole Directed Ring Assembly of Ni-Coated Au-Nanorods. *Chem. Commun.* **2010**, *46* (36), 6711–6713.

(81) Xing, Z.-H.; Wang, S.-S.; Xu, A.-W. Dipole-Directed Assembly of Fe3O4 Nanoparticles into Nanorings Via Oriented Attachment. *CrystEngComm* **2014**, *16* (8), 1482–1487.

(82) Allia, P.; Coisson, M.; Tiberto, P.; Vinai, F.; Knobel, M.; Novak, M.; Nunes, W. Granular Cu-Co Alloys as Interacting Superparamagnets. *Phys. Rev. B* **2001**, *64* (14), No. 144420.

(83) Ji, H.; Trevino, J.; Tu, R.; Knapp, E.; McQuade, J.; Yurkiv, V.; Mashayek, F.; Vuong, L. T. Long-Range Self-Assembly via the Mutual Lorentz Force of Plasmon Radiation. *Nano Lett.* **2018**, *18* (4), 2564–2570.

(84) Sheikholeslami, M.; Arabkoohsar, A.; Khan, I.; Shafee, A.; Li, Z. Impact of Lorentz Forces on Fe3O4-Water Ferrofluid Entropy and Exergy Treatment within a Permeable Semi Annulus. *J. Clean. Prod.* **2019**, *221*, 885–898.

(85) Wang, Z.; Holm, C. Estimate of the Cutoff Errors in the Ewald Summation for Dipolar Systems. *J. Chem. Phys.* **2001**, *115* (14), 6351–6359.

(86) Mahmood, A. LAMMPS MSPIN Plugin. https://github.com/yingling-group/lammps-mspin (accessed Nov 15, 2021).

(87) Fleet, M. E. The Structure of Magnetite. http://crystallography.net/cod/9007644.html (accessed May 16, 2019).

(88) Macrae, C. F.; Edgington, P. R.; McCabe, P.; Pidcock, E.; Shields, G. P.; Taylor, R.; Towler, M.; Streek, J. van de. Mercury: Visualization and Analysis of Crystal Structures. *J. Appl. Crystallogr.* **2006**, *39* (3), 453–457.

(89) Case, D. A.; Cheatham, T. E.; Darden, T.; Gohlke, H.; Luo, R.; Merz, K. M.; Onufriev, A.; Simmerling, C.; Wang, B.; Woods, R. J. The Amber Biomolecular Simulation Programs. *J. Comput. Chem.* **2005**, *26* (16), 1668–1688.

(90) Tombácz, E.; Farkas, K.; Földesi, I.; Szekeres, M.; Illés, E.; Tóth, I. Y.; Nesztor, D.; Szabó, T. Polyelectrolyte Coating on Superparamagnetic Iron Oxide Nanoparticles as Interface Between Magnetic Core and Biorelevant Media. *Interface Focus* **2016**, *6* (6), No. 20160068.

(91) Rappe, A. K.; Casewit, C. J.; Colwell, K. S.; Goddard, W. A.; Skiff, W. M. Uff, a Full Periodic Table Force Field for Molecular Mechanics and Molecular Dynamics Simulations. *J. Am. Chem. Soc.* **1992**, *114* (25), 10024–10035.

(92) Bixner, O.; Lassenberger, A.; Baurecht, D.; Reimhult, E. Complete Exchange of the Hydrophobic Dispersant Shell on Monodisperse Superparamagnetic Iron Oxide Nanoparticles. *Langmuir* **2015**, *31* (33), 9198–9204.

(93) Schmidt, M. W.; Baldridge, K. K.; Boatz, J. A.; Elbert, S. T.; Gordon, M. S.; Jensen, J. H.; Koseki, S.; Matsunaga, N.; Nguyen, K. A.; Su, S.; Windus, T. L.; Dupuis, M.; Montgomery, J. A. General Atomic and Molecular Electronic Structure System. *J. Comput. Chem.* **1993**, *14* (11), 1347–1363.

(94) Bayly, C. I.; Cieplak, P.; Cornell, W.; Kollman, P. A. A Well-Behaved Electrostatic Potential Based Method Using Charge Restraints for Deriving Atomic Charges: The Resp Model. *J. Phys. Chem.* **1993**, *97* (40), 10269–10280.

(95) Dupradeau, F.-Y.; Pigache, A.; Zaffran, T.; Savineau, C.; Lelong, R.; Grivel, N.; Lelong, D.; Rosanski, W.; Cieplak, P. The R.E.D. Tools: Advances in RESP and ESP Charge Derivation and Force Field Library Building. *Phys. Chem. Chem. Phys.* **2010**, *12* (28), 7821–7839.

(96) Wang, J.; Wolf, R. M.; Caldwell, J. W.; Kollman, P. A.; Case, D. A. Development and Testing of a General Amber Force Field. *J. Comput. Chem.* **2004**, *25* (9), 1157–1174.

(97) Plimpton, S. Fast Parallel Algorithms for Short-Range Molecular Dynamics. *J. Comput. Phys.* **1995**, *117* (1), 1–19.

(98) Hockney, R. W.; Eastwood, J. W. *Computer Simulation Using Particles*; CRC Press, 1988.

(99) Hoover, W. G. Canonical Dynamics: Equilibrium Phase-Space Distributions. *Phys. Rev. A* **1985**, *31* (3), 1695–1697.

(100) Li, N. K.; Xie, Y.; Yingling, Y. G. Insights into Structure and Aggregation Behavior of Elastin-like Polypeptide Coacervates: All-Atom Molecular Dynamics Simulations. *J. Phys. Chem. B* **2021**, *125* (30), 8627–8635.

(101) Lee, H.; Stryutsky, A.; Mahmood, A.-U.; Singh, A.; Shevchenko, V. V; Yingling, Y. G.; Tsukruk, V. V. Weakly Ionically Bound Thermosensitive Hyperbranched Polymers. *Langmuir* **2021**, *37* (9), 2913–2927.

(102) Oweida, T. J.; Kim, H. S.; Donald, J. M.; Singh, A.; Yingling, Y. G. Assessment of AMBER Force Fields for Simulations of SsDNA. *J. Chem. Theory Comput.* **2021**, *17* (2), 1208–1217.

(103) Singh, A.; Kwansa, A. L.; Kim, H. S.; Williams, J. T.; Yang, H.; Li, N. K.; Kubicki, J. D.; Roberts, A. W.; Haigler, C. H.; Yingling, Y. G. In Silico Structure Prediction of Full-Length Cotton Cellulose Synthase Protein (GhCESA1) and Its Hierarchical Complexes. *Cellulose* **2020**, *27* (10), 5597–5616.

(104) Humphrey, W.; Dalke, A.; Schulten, K. VMD: Visual Molecular Dynamics. *J. Mol. Graphics* **1996**, *14* (1), 33–38.

(105) Roe, D. R.; Cheatham, T. E. PTRAJ and CPPTRAJ: Software for Processing and Analysis of Molecular Dynamics Trajectory Data. *J. Chem. Theory Comput.* **2013**, *9* (7), 3084–3095.

FIGURE FOR TABLE OF CONTENTS ONLY: